Model Predictive Frequency Control of Low Inertia Microgrids

Ujjwol Tamrakar†, Timothy M. Hansen,
and Reinaldo Tonkoski
Department of Electrical Engineering and Computer Science
South Dakota State University
Brookings, South Dakota, USA
Email: †ujjwol.tamrakar@jacks.sdstate.edu

David A. Copp
Sandia National Laboratories
Albuquerque, New Mexico, USA

***Abstract*—In isolated power systems with low rotational inertia, fast-frequency control strategies are required to maintain frequency stability. Furthermore, with limited resources in such isolated systems, the deployed control strategies have to provide the flexibility to handle operational constraints so the controller is optimal from a technical as well as an economical point-of-view. In this paper, a model predictive control (MPC) approach is proposed to maintain the frequency stability of these low inertia power systems, such as microgrids. Given a predictive model of the system, MPC computes control actions by recursively solving a finite-horizon, online optimization problem that satisfies peak power output and ramp-rate constraints. MATLAB/Simulink based simulations show the effectiveness of the controller to reduce frequency deviations and the rate-of-change-of-frequency (ROCOF) of the system. By proper selection of controller parameters, desired performance can be achieved while respecting the physical constraints on inverter peak power and/or ramp-rates.**

***Index Terms*—Fast frequency control, frequency stability, model predictive control, virtual inertia**

I. Introduction

This paper focuses on fast-frequency control of low inertia, inverter-dominated microgrids. Typically, remote microgrids have a relatively low amount of rotational generation. Frequency control in these microgrids is difficult due to the fast-frequency dynamics that occur during a transient event. Inverter-based renewable generation does not contribute to system inertia, which makes the system susceptible to large frequency swings in a short time interval as there is limited inertial response to counteract the frequency change. Even if a system has adequate reserve, the slow-acting nature of these traditional reserves may not be able to handle high rate-of-change-of-frequency (ROCOF), which compromises the frequency stability of the system [1]. Another effect of increased penetration of variable generation is that it affects the number of synchronous generators that are online at any given time. The inertia of the power system can thus vary based on the number of generators that are online [2]. This uncertainty further complicates the design of the frequency controller. Hence, there is a need to develop optimal and effective fast-acting frequency controllers.

Traditionally, to compensate these fast-frequency variations, inverters have been equipped with algorithms that dispatch power based on the derivative of the frequency measurements. This allows the inverter to react very fast in response to frequency changes [3]. Energy storage systems (ESSs) can be utilized to provide the power needed for such fast-frequency services [4]. Classic PID based control techniques are used to control these inverters. As such, it is difficult to incorporate constraints on power limits and ramp-rates with such controllers. Moreover, tuning of these controllers is not intuitive, and it is difficult to relate the physical behavior (like inertia emulation, damping and/or peak power) of the system with the control parameters. Model predictive controllers (MPCs) can optimize the behavior of these controllers as desired based on the system operating conditions [5]. Furthermore, such a control approach has the added flexibility of incorporating other constraints, such as power limits and ramp-rate limits, that have economic impacts. MPC design is based on tuning a few weighting parameters that are easily relatable to the physical behavior of the system as will be illustrated later.

In [6], a control scheme was developed to adaptively select the gains of the controller online based on an underlying model to reduce the energy exchange with the ESS. However, the controller only had the capability to predict one time-step ahead. An explicit MPC approach for fast-frequency control was proposed in [7]. In this implementation, the solutions are analytically computed offline, and the control action reduces to a lookup table. Linear quadratic regulator (LQR) based optimal controllers have also been developed in literature with an aim of achieving an optimal controller [8], [9]. However, optimization is performed offline, and the controller may not perform "optimally" if system dynamics vary. Furthermore, there is no explicit method to incorporate operational constraints in the LQR controller formulation. Apart from these model-based approaches, a few model free methods have also been explored in the literature based on reinforcement learning [10], [11] and fuzzy logic [12]. However, such methods may require intensive training and online computation power, which may not be feasible. In this paper, an online MPC approach is proposed for fast-frequency control based on a long time horizon that provides near-optimal control actions based on system operating conditions. In addition, the proposed MPC approach utilizes an objective function that enables the possibility of providing both inertial response and frequency regulation within the same

MPC formulation for power system fast-frequency control.

The paper is organized as follows: Section II develops a model for the frequency dynamics of an isolated power system followed by a description of the proposed MPC formulation. In Section III, the methods and procedures are described for the simulation study. The results and findings are presented in Section IV, and Section V concludes the paper.

II. MPC-based Frequency Control

In this section, a generic model for the frequency dynamics of a power system is derived, followed by the MPC formulation for frequency control.

A. Frequency Event Characterization

When a frequency event (power imbalance) occurs in a power system, the frequency of the system deviates from its steady-state value. Fig. 1 shows how the frequency of a typical power system evolves after a frequency event. In this case, an increase in the net electrical load in the system has caused the frequency to drop. The initial rate-of-change-of-frequency (ROCOF) depends on the total inertia available in the system [13]. In isolated power systems, this inertia can be particularly low and can cause large ROCOF that may trigger frequency relays, which can cut-off the generator. Based on this initial rate-of-change, the frequency reaches a nadir ω_{nadir} after a time t_n from the start of the frequency event. The maximum ROCOF is denoted by $\dot{\omega}_{max}$ in Fig. 1. For these initial few seconds, the inertial response is entirely responsible for maintaining power balance. After this, governors start acting on the system to stabilize the frequency and reduce the steady-state error. The time taken for the frequency to return to its steady-state value is defined as the recovery/settling time.

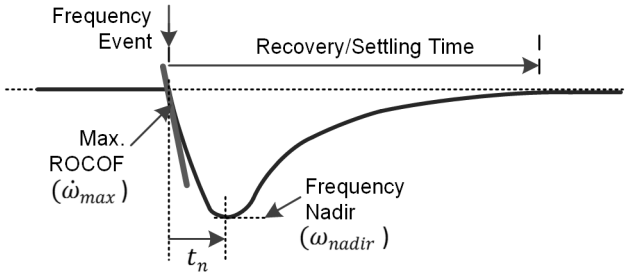

Fig. 1: Power system frequency after a frequency event.

B. System Model

The frequency dynamics of an isolated power system can be modeled based on the so-called *swing equation* and a differential equation representing the dynamics of the governor as follows [9], [14]:

$$M\dot{\Delta\omega} + D\Delta\omega = \Delta P_m - \Delta P_e \tag{1}$$

$$T_g\Delta\dot{P}_m + \Delta P_m = -R_p^{-1}\Delta\omega \tag{2}$$

where M represents the equivalent inertia constant of the generator, D is the normalized damping constant (which accounts for the equivalent effect of all frequency dependent loads in the system), ω is the system frequency, and P_m and P_e represent the mechanical power and the electrical power, respectively. Similarly, T_g and R_p are the time constant and the equivalent speed regulation droop. Fig. 2 shows a block diagram of the power system defined by (1) and (2). To reduce the frequency deviation to zero in the steady-state, an integral control loop with a power output of ΔP_s is also added. K_i represents the integral gain of this secondary control loop. For the design of controllers which emulate inertia, the dynamics of this slower secondary control loop can be neglected [8]. From the point-of-view of dynamic frequency control, the secondary power output ΔP_s does not have a significant impact.

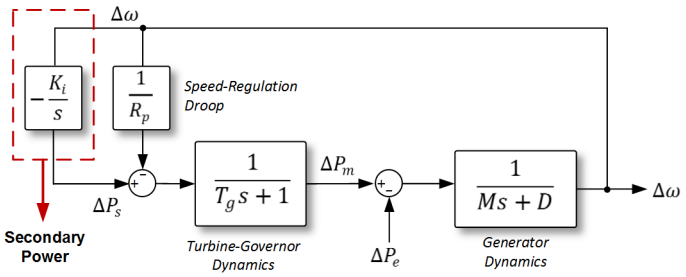

Fig. 2: Block diagram of the isolated power system.

Based on (1) and (2), the following differential equation can be derived:

$$\ddot{\Delta\omega} = -\left(\frac{D}{M} + \frac{1}{T_g}\right)\dot{\Delta\omega} - \left(\frac{D}{MT_g} + \frac{1}{R_pMT_g}\right)\Delta\omega - \frac{1}{MT}\Delta P_e - \frac{\Delta P_e}{M}. \tag{3}$$

The state-space representation of the differential equation is given by:

$$\begin{bmatrix}\dot{\Delta\omega}\\ \ddot{\Delta\omega}\end{bmatrix} = \begin{bmatrix}0 & I\\ -\left(\frac{D}{MT_g} + \frac{1}{R_pMT_g}\right) & -\left(\frac{D}{M} + \frac{1}{T_g}\right)\end{bmatrix}\begin{bmatrix}\Delta\omega\\ \dot{\Delta\omega}\end{bmatrix} + \begin{bmatrix}0\\ \frac{-1}{MT_g}\end{bmatrix}\Delta P_e \tag{4}$$

C. Proposed Model Predictive Controller

An MPC approach is proposed in this paper for fast-frequency control of an isolated power system. In particular, the objective of the controller is to emulate inertial response during the first few seconds after a frequency event. The proposed controller can act much faster than the frequency controllers in a traditional power system to reduce the initial ROCOF. Fig. 3 shows a schematic diagram of the proposed MPC. The frequency and ROCOF measurements are sent to the MPC, which computes a sequence of future control actions by minimizing a desired cost function given a predictive model of the system and system constraints. In MPC, the first control action in this sequence is applied, and the optimization is solved again at each subsequent time step in a receding horizon fashion.

The set $\mathcal{T} := \{t, t+\tau, ..., t+T-\tau\}$ is defined as the discrete times in the finite forward time horizon. T is defined as the length of the time horizon, which is a multiple of the time step τ. Defining $x_k = [\Delta\omega_k \ \dot{\Delta\omega_k}]^\top$ as the discrete states of the system and Δp_k as the power output from the virtual inertia unit, the proposed MPC formulation will take the following form:

$$\text{minimize } J = \sum_{k=t}^{t+T-\tau} \left(x_k^\top Q x_k + \Delta p_k^\top R \Delta p_k\right) + x_{t+T}^\top Q^f x_{t+T} \tag{5a}$$

subject to

$$x_{k+\tau} = Ax_k + B\Delta p_k \quad \forall k \in \mathcal{T}, \tag{5b}$$

$$|\Delta p_k| \leq P_{max} \quad \forall k \in \mathcal{T}, \tag{5c}$$

$$\|\Delta p_{k+\tau} - \Delta p_k\|_\infty \leq S \quad \forall k \in \mathcal{T}, \tag{5d}$$

where A and B are the discretized state-space matrices of the system. The discretization is performed using the zero order hold (ZOH) method with a sampling time of τ. J is the cost-function to be minimized, and Q and R are the weighting matrices corresponding to the state estimates and the control input respectively. The weighting matrix Q can be used to penalize poor system performance (i.e., to penalize change in frequency and/or ROCOF), while matrix R is used to penalize the control effort (i.e., the power output from the inverter). The weighting matrix Q is defined as:

$$Q = \begin{bmatrix} Q_{11} & 0 \\ 0 & Q_{22} \end{bmatrix}. \tag{6}$$

Similarly, Q^f is a terminal cost weighting matrix. We assume that Q^f is equal to Q throughout the paper. More details on the choice of the terminal cost and time horizon can be found in [15].

Solving this optimal control problem over the time horizon $\mathcal{T}$ results in the solution $\Delta p^* := [\Delta p_t{}^*, \Delta p_{t+\tau}{}^*, ..., \Delta p_{t+T-\tau}{}^*]$. At each time t, the first element of the solution Δp^* is used which gives the following control law:

$$\Delta p_t = \Delta p_t{}^*. \tag{7}$$

The system dynamics are incorporated within the constraint (5b) of the above MPC formulation. Similarly, (5c) limits the power output of the inverter to P_{max}. The ramp-rate of the inverter power output is limited to S by (5d).

III. Methodology

The simulation studies were carried out in MATLAB/Simulink. The simulation setup used is illustrated in Fig. 4. The system is based on the PV-Hydro model described in [16]. It consists of a 39 kVA hydro system and a 25 kWp PV system. In this paper, we model the generator and develop the MPC approach to provide fast-frequency control. A generator driven by a turbine is the main power source controlling the voltage and the frequency of the system. A variable load is also connected to the system. Whenever the load changes, variations occur in the system frequency, which are traditionally regulated by the governor. In this case, the inverter (marked as virtual inertia unit in Fig. 4) provides faster frequency response based on the MPC that was formulated in Section II-C.

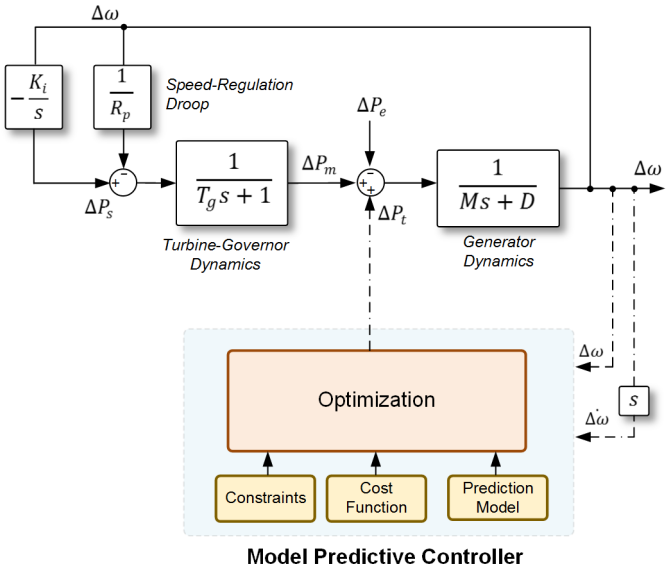

Fig. 3: Block diagram of the power system model with the MPC approach.

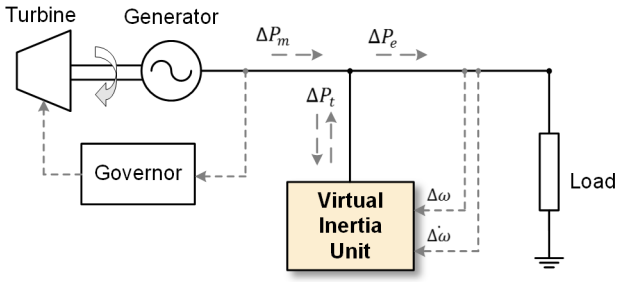

Fig. 4: Simulation setup used in MATLAB/Simulink.

It should be noted that Fig. 4 is only used as an illustration of the system under study, and the simulations are carried out using state-space blocks in MATLAB/Simulink. The parameters used in the simulation are typical values and are summarized in Table I.

TABLE I: Summary of Simulation Parameters

Parameter	Values
Inertia constant (M)	4 s
Damping coefficient (D)	1.5%
Speed regulation droop (R_p)	5%
Turbine-Governor time constant (T_g)	0.2 s
Sample time (τ)	0.02 s
Prediction and Control Horizon (T)	1 s

The MPC approach was implemented in MATLAB/Simulink using CVXGEN, a code generator for

embedded convex optimization [17]. CVXGEN generates C code that is compiled into high speed solvers [18]. When incorporated with MATLAB, CVXGEN creates a MATLAB MEX (MATLAB executable) interface to be used within Simulink to call the custom solver.

IV. Results and Analysis

In this section, the frequency dynamics of the benchmark presented in Section III is studied under different configurations of the MPC formulation. Based on how the weighting matrices are selected, the frequency dynamics of the benchmark power system varies significantly. Initially, the effect of changing Q_{11} and Q_{22} is studied independently followed by a series of simulations that are utilized to select the best combination of Q_{11} and Q_{22}. The constrained operation of the MPC formulation is also analyzed. Finally, a short discussion on the computation time is provided.

A. Minimizing the Rate-of-Change-of-Frequency (ROCOF)

In this first case study, the objective of the MPC is to minimize the ROCOF of the system. For this, Q_{11} is always set to 0 and Q_{22} is varied from 0.1 to 1. R is set to a small value of 0.001 indicating a small penalty on the control action. P_{max} was set to 1.0 p.u. and the maximum ramp-rate, S, was set to 10 p.u./s. These values were intentionally chosen large so that the constraints do not become active. The cost function is now reduced to the following form:

$$J = \sum_{k=t}^{t+T-\tau} \left\{ Q_{22} \Delta \dot{\omega}_k{}^2 + R(\Delta p_k)^2 \right\} \tag{8}$$

Fig. 5 shows the change in frequency and the ROCOF for these MPC settings. Increasing Q_{22} minimizes the ROCOF of the system. The peak power injection from the inverter also increases accordingly. However, it is interesting to note that the frequency nadir has increased. Increasing the Q_{22} parameter tries to reduce the ROCOF without any damping in the system. This creates an overshoot in the ROCOF that causes a negative spike in the power output from the inverter, causing the frequency nadir to increase even more than in the case with no controller. This behavior is similar to adding inertia to the system.

B. Minimizing the Change in Frequency

In the second case study, the objective of the MPC is to minimize the change in the frequency. For this, Q_{22} is always set to 0 and Q_{11} is varied from 0.1 to 1. The remaining parameters are the same as in the first case study. In this case, the cost function is reduced to the following form:

$$J = \sum_{k=t}^{t+T-\tau} \left\{ Q_{11} \Delta \omega_k{}^2 + R(\Delta p_k)^2 \right\} \tag{9}$$

Fig. 6 shows the change in frequency and the ROCOF for these MPC settings. As expected, increasing Q_{11} reduces the frequency nadir of the system. Although there is a significant amount of damping added to the system, the frequency dynamics are not slower as desired. It can also be observed that the

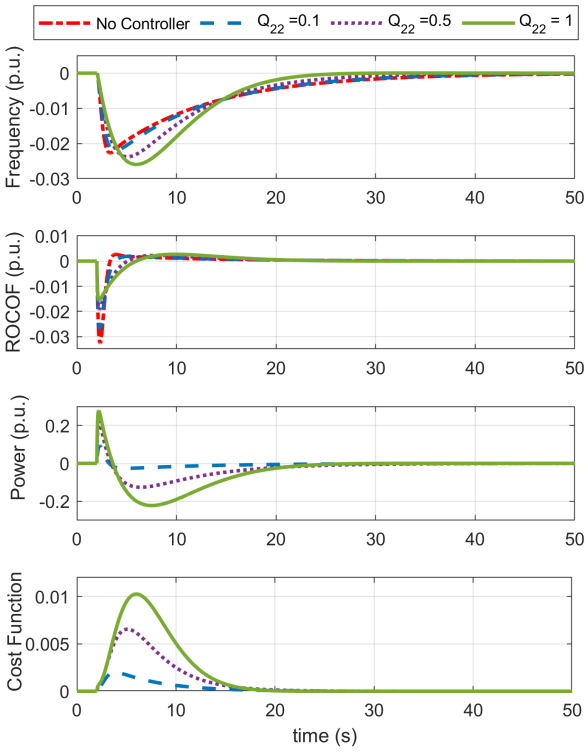

Fig. 5: Frequency and ROCOF when varying Q_{22} keeping $Q_{11} = 0$.

reduction in the ROCOF is not as significant as in the previous case. As a consequence, the time-to-nadir remains relatively unchanged. Hence, increasing Q_{11} has a behavior similar to adding more damping to the system. Based on this discussion, it is clear that a suitable combination of Q_{11} and Q_{22} would be needed to achieve the desired performance where both frequency nadir and ROCOF are reduced to a desirable level.

C. Minimizing Both Change in Frequency and ROCOF

In this case, both Q_{11} and Q_{22} are chosen to analyze the combined effect of these parameters in the MPC performance. Repeated simulations were carried out varying both Q_{11} and Q_{22} in the range of $[0.1,\ 1]$ at intervals of 0.1. The data obtained from these simulations are summarized using heat-maps. Fig. 7 shows the heat-maps for variations of minimum frequency point ω_{nadir} and maximum ROCOF $\dot{\omega}_{max}$. It can be observed from Fig. 7 that increasing either Q_{11} or Q_{22} reduces the frequency deviation, except at lower values of Q_{11}. When Q_{11} is low, at high values of Q_{22}, the frequency nadir gets worse compared to the no MPC case. In case of the heat-map for ROCOF, increasing Q_{22} has a significant impact in decreasing the ROCOF. An increase in Q_{11} has a similar effect, but the impact is less significant.

Similarly, the effect of varying Q_{11} and Q_{22} on the time-to-nadir t_n and the peak power injection Δp is shown in Fig. 8. The time-to-nadir should ideally be as high as possible, as it indicates that the frequency dynamics have slowed. This allows time for the governor response from the synchronous generators to act and return the system frequency to steady-

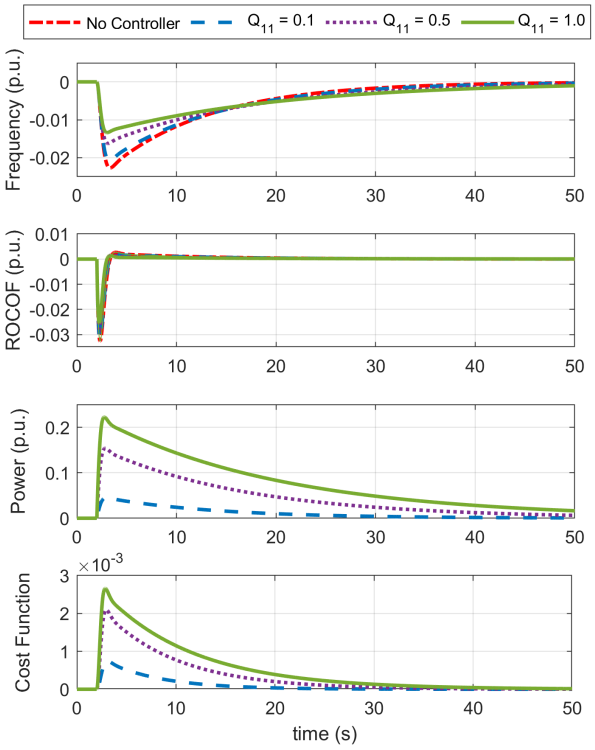

Fig. 6: Frequency and ROCOF when varying Q_{11} keeping $Q_{22} = 0$.

state. The time-to-nadir is highest when $Q_{22} = 1$ and $Q_{11} = 0$, although increasing Q_{11} does not significantly reduce the time-to-nadir at higher ranges of Q_{22}. The peak inverter power is maximum when Q_{11} and Q_{22} are set to 1. This is as expected, because the highest peak power would be required when both frequency deviation and ROCOF are penalized equally with the highest weights. Based on these heat maps, the point $(Q_{22} = 0.5, Q_{11} = 0.7)$ is a good choice because it provides a fair compromise between reducing the frequency nadir and ROCOF. At this point, the time-to-nadir is fairly high at 2.5–3.0s, and peak power injection is about 10 kW. If a lower power injection is desired, Q_{11} could be reduced further. From this study, it is clear that appropriate selection of the weighting matrices provides an intuitive technique to tune system performance as desired.

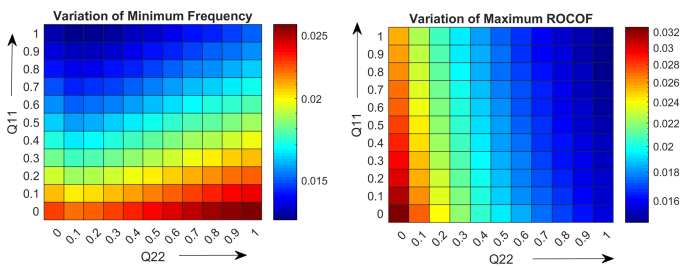

Fig. 7: Heat-map showing the effect of varying Q_{11} and Q_{22} on the change in frequency and the ROCOF if the system.

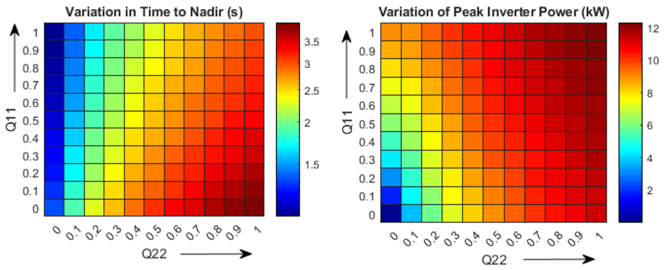

Fig. 8: Heat-map showing the effect of varying Q_{11} and Q_{22} on the time to frequency nadir t_n and peak power injection Δp.

D. Constrained Operation with MPC

In this section, the ability of the MPC approach to incorporate constraints is highlighted. Using the $(Q_{22} = 0.5, Q_{11} = 0.7)$ from the previous section, the performance is compared when limits are imposed on the maximum power output and the ramp-rate of the MPC. In this particular case, the peak inverter power is limited to 0.15 p.u. (6 kW), and the ramp-rate is limited to 0.5 p.u./s (1 kW/s). These constraints indicate that in a real system the inverter peak power is limited to 6 kW, and 1 kW/s is the allowable ramp-rate for the type of energy storage system being used. Fig. 9 shows the performance of the constrained MPC versus the unconstrained MPC approach. With a constraint on peak power, the output power from the inverter is limited to 0.15 pu, and the change in the power is limited by the ramp-rate constraint. However as a compromise, the frequency nadir and the ROCOF are higher compared to the unconstrained case. Also, the time to frequency nadir is much smaller in the constrained case.

The ability to include constraints with the proposed MPC approach can provide a means for microgrid operators to incorporate inertial response services based on the requirement of the end-users. The constraints can be adjusted based on whether the criteria such as maximum allowable ROCOF and/or frequency nadir is high or low. Based on this the microgrid operators can then add value to the type of energy storage needed and/or the lifetime of the energy storage being used.

E. Discussion on the Computation Time

To highlight the computational feasibility of the MPC approach in a real-time controller, the MPC solver in CVXGEN was run for 100 trials (the MPC optimized over the given horizon) using MATLAB. The trials were conducted on a Intel Core i7 - 8750H processor operating at 2.2 GHz. The total execution time of the 100 trials was calculated as 40 ms using the MATLAB profiler, which is an average of 400 μs per trial. Although the execution time may increase when implementing the MPC solver in a low cost embedded controller, as one trial is well under the sampling time of 20 ms the real-time implementation of the MPC controller is shown to be feasible in this initial analysis.

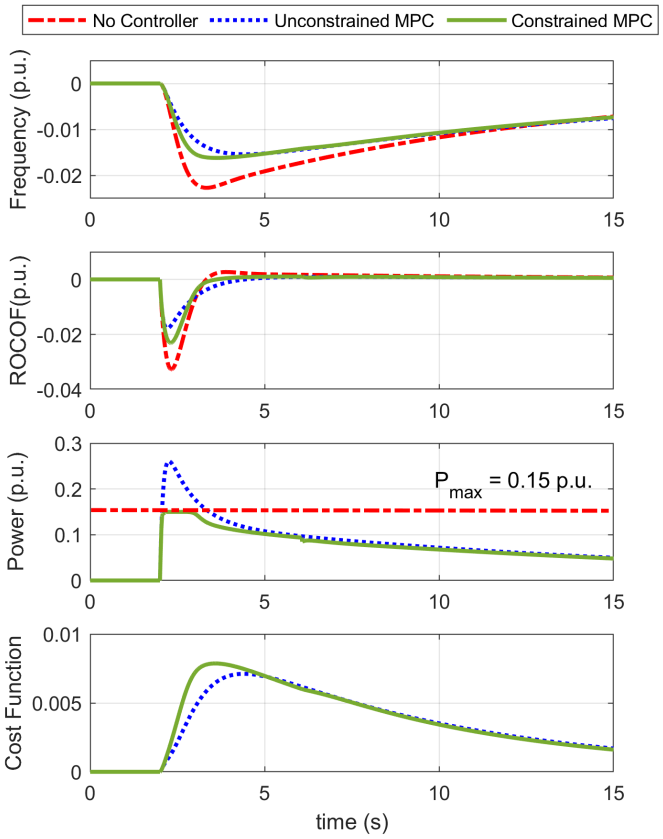

Fig. 9: Comparison of constrained and unconstrained MPC approach.

V. Conclusions and Future Work

An MPC approach was developed to provide fast-frequency control for an isolated power system. The inverter was able to act faster than the governor of the system to counteract the power imbalance. This allowed the system to achieve low ROCOF and frequency deviations. It was also found that with appropriate selection of MPC parameters, the frequency behavior and the power from the inverter can be intuitively controlled. In this sense, the MPC provides a flexible framework to control the system frequency as per operator requirements, while simultaneously considering the cost and underlying constraints of the physical system. The choice of the MPC time-step and time-horizon will depend largely on the computational power of the controller being used and will be analyzed in future. Furthermore, the possibility of providing both inertial response and frequency regulation with the same MPC formulation will also be explored as a part of future work.

Acknowledgment

This work is supported by the National Science Foundation (NSF) under Grant Number MRI-1726964 and US DOE Energy Storage Program managed by Dr. Imre Gyuk of the DOE Office of Electricity Delivery and Energy Reliability.

Sandia National Laboratories is a multi-mission laboratory managed and operated by National Technology and Engineering Solutions of Sandia, LLC., a wholly owned subsidiary of Honeywell International, Inc., for the U.S. Department of Energy National Nuclear Security Administration under contract DE-NA-0003525.

References

[1] IEEE PES Task Force on Microgrid Stability Analysis and Modeling, "Microgrid Stability Definitions, Analysis, and Modeling," IEEE, Tech. Rep., 2018.

[2] G. S. Misyris, S. Chatzivasileiadis, and T. Weckesser, "Robust frequency control for varying inertia power systems," in *IEEE PES Innovative Smart Grid Technologies Conference Europe (ISGT-Europe)*. IEEE, 2018, 6 pp.

[3] H.-P. Beck and R. Hesse, "Virtual synchronous machine," in 9^{th} *International Conference on Electrical Power Quality and Utilisation*, 2007, 6 pp.

[4] R. H. Byrne, T. A. Nguyen, D. A. Copp, B. R. Chalamala, and I. Gyuk, "Energy management and optimization methods for grid energy storage systems," *IEEE Access*, vol. 6, pp. 13 231–13 260, 2018.

[5] D. Q. Mayne, J. B. Rawlings, C. V. Rao, and P. O. Scokaert, "Constrained model predictive control: Stability and optimality," *Automatica*, vol. 36, no. 6, pp. 789–814, 2000.

[6] M. A. Torres L, L. A. Lopes, L. A. Moran T, and J. R. Espinoza C, "Self-tuning virtual synchronous machine: a control strategy for energy storage systems to support dynamic frequency control," *IEEE Transactions on Energy Conversion*, vol. 29, pp. 833–840, 2014.

[7] A. Ulbig, T. Rinke, S. Chatzivasileiadis, and G. Andersson, "Predictive control for real-time frequency regulation and rotational inertia provision in power systems," in *IEEE* 52^{nd} *Annual Conference on Decision and Control (CDC)*, 2013, pp. 2946–2953.

[8] M. Torres and L. A. Lopes, "An optimal virtual inertia controller to support frequency regulation in autonomous diesel power systems with high penetration of renewables," in *Proceedings of the International Conference on Renewable Energies and Power Quality (ICREPQ 11), la Palmas de Gran Canaria, Spain*, 2011, pp. 13–15.

[9] U. Markovic, Z. Chu, P. Aristidou, and G. Hug, "Fast frequency control scheme through adaptive virtual inertia emulation," in *Proceedings of the IEEE PES ISGT Asia*, 2018.

[10] W. Guo, F. Liu, J. Si, and S. Mei, "Incorporating approximate dynamic programming-based parameter tuning into pd-type virtual inertia control of dfigs," in *International Joint Conference on Neural Networks (IJCNN)*, 2013, 8 pp.

[11] D. Shrestha, U. Tamrakar, N. Malla, Z. Ni, and R. Tonkoski, "Reduction of energy consumption of virtual synchronous machine using supplementary adaptive dynamic programming," in *IEEE International Conference on Electro Information Technology (EIT)*, May 2016, pp. 0690–0694.

[12] H. R. Chamorro, I. Riano, R. Gerndt, I. Zelinka, F. Gonzalez-Longatt, and V. K. Sood, "Synthetic inertia control based on fuzzy adaptive differential evolution," *International Journal of Electrical Power & Energy Systems*, vol. 105, pp. 803–813, 2019.

[13] F. Milano, F. Dörfler, G. Hug, D. J. Hill, and G. Verbič, "Foundations and challenges of low-inertia systems," in *Power Systems Computation Conference (PSCC)*, 2018, 25 pp.

[14] P. Kundur, N. J. Balu, and M. G. Lauby, *Power system stability and control*. McGraw-hill New York, 1994, vol. 7.

[15] G. Grimm, M. J. Messina, S. E. Tuna, and A. R. Teel, "Model predictive control: for want of a local control lyapunov function, all is not lost," *IEEE Transactions on Automatic Control*, vol. 50, no. 5, pp. 546–558, May 2005.

[16] U. Tamrakar, D. Galipeau, R. Tonkoski, and I. Tamrakar, "Improving transient stability of photovoltaic-hydro microgrids using virtual synchronous machines," in *IEEE PowerTech*, 2015, 6pp.

[17] "CVXGEN: Code Generation for Convex Optimization," https://cvxgen.com/docs/index.html, Accessed: 01-08-2019.

[18] J. Mattingley and S. Boyd, "CVXGEN: a code generator for embedded convex optimization," *Optimization and Engineering*, vol. 13, no. 1, pp. 1–27, 2012.